Journal of Photochemistry and Photobiology 24 (2024) 100252

Contents lists available at ScienceDirect

Journal of Photochemistry and Photobiology

journal homepage: www.sciencedirect.com/journal/journal-of-photochemistry-and-photobiology

Strategies for overcoming the lung surfactant barrier and achieving success in antimicrobial photodynamic therapy

Isabelle Almeida de Lima [a,*], Lorraine Gabriele Fiuza [a], Johan Sebastián Díaz Tovar [a], Dianeth Sara Lima Bejar [a], Ana Julia Barbosa Tomé [a], Michelle Barreto Requena [a,b], Layla Pires [c], Gang Zheng [c], Natalia Mayumi Inada [a], Cristina Kurachi [a], Vanderlei Salvador Bagnato [a,b]

[a] São Carlos Institute of Physics, University of São Paulo, São Carlos, SP, Brazil
[b] Department of Biomedical Engineering, Texas A&M University, USA
[c] Princess Margaret Cancer Centre, University Health Network, Toronto, Canada

ARTICLE INFO

Keywords:
Pneumonia
Lung surfactant
Indocyanine green
Infrared light
Antimicrobial photodynamic therapy

ABSTRACT

The impressive increase in antimicrobial resistance has required the development of alternative treatments that act on multiple non-specific molecular targets and are effective against a broad range of microorganisms. Antimicrobial Photodynamic Therapy (aPDT) is based on microbial inactivation from oxidative stress and represents an important tool for inactivating microorganisms with low risk of resistance selection. Therefore, our research group has been devoted to demonstrating its effectiveness against pathogens that cause pneumonia, one of the most lethal infections worldwide. Previous studies reported the efficiency and safety of an *in vitro* photoinactivation protocol for *Streptococcus pneumoniae* and the delivery of infrared light (external illumination) and photosensitizer (PS) in an animal model. However, the *in vivo* inactivation of microorganisms still poses challenges due to the presence of lung surfactant (LS), which traps PSs, preventing them from reaching the microbial target. This study investigated different approaches such as use of emulsifiers, perfluorocarbon, oxygen nanobubbles, and copolymer towards overcoming LS and optimizing aPDT response. The most promising strategy consisted in combining indocyanine green (ICG) with Gantrez^{TM} AN-139 - a Polyvinyl Methyl Ether/Maleic Anhydride copolymer (PVM/MA) – showing high microbial inactivation and safety for human lung epithelial (A549) and fibroblast (MRC-9) cell lines. The *in vitro* experiments provided an alternative to overcome the limited PS distribution through LS and will serve as the basis for *in vivo* studies.

1. Introduction

Lower respiratory tract infections (LRTIs) are the fifth leading cause of death worldwide, with pneumococcal pneumonia accounting for nearly 60 % of cases and resulting in approximately 2.2 million deaths in 2021. This infection represents a significant medical and economic burden due to the costs associated with prolonged hospitalization and long-term consequences, such as potential reductions in lung function and recurrence of secondary infections [1–3]. The situation is alarming due to the rapid emergence of new resistant microorganism strains and the limitation of pharmaceutical companies to develop new therapeutics in short time, highlighting the urgent need for approaches with broad applicability [4]. Among such approaches, antimicrobial photodynamic therapy based on the combination of a photosensitizer, light, and oxygen, stands out. When illuminated at an appropriate wavelength and in presence of molecular oxygen, the photosensitizer is activated, leading to the formation of reactive oxygen species (ROS) that cause cell death [5,6]. Its advantages include a broad spectrum of action, double selectivity (PS and light can be administered locally), non-invasive nature, and no cumulative toxic effects. Moreover, one of the most relevant aspects in the context of this study is the low probability of selecting resistant microorganisms [7,8]. The promising recent reports of aPDT breaking down the resistance of some bacteria species have also justified its development for a possible treatment combined with antibiotics [9, 10].

Over the past ten years, our research group has proposed using aPDT for lung disinfection (Fig. 1) and reported ICG-mediated aPDT can inactivate *S. pneumonieae in vitro* while preserving RAW 264.7 murine

* Corresponding author.
E-mail addresses: isabelle.almeida016@gmail.com (I.A. de Lima), vander@ifsc.usp.br (V.S. Bagnato).

https://doi.org/10.1016/j.jpap.2024.100252

Available online 25 September 2024

macrophages [11]. Later and in a murine model, Kassab *et al.* demonstrated nebulization successfully delivered photosensitizers to the respiratory tract [12]. Tovar *et al.* used an *ex vivo* pig thoracic carcass model to demonstrate the feasibility of external illumination and showed ICG activation and *S. pneumoniae* inactivation upon external illumination [13]. aPDT has also been proposed for the treatment of other pneumonia-causing pathogens, including those on the World Health Organization (WHO) priority list for which new antibiotics are urgently required due to increasing microbial resistance. Those include *S. aureus* (methicillin-resistant), *K. pneumoniae* (multi-resistant), and *P. aeruginosa* (multi-resistant), which have shown susceptible to photodynamic inactivation through different PSs (*e.g.*, porphyrins, toluidine blue, ICG, methylene blue, among others) in *in vitro* studies [14–18].

Despite the great potential of the photodynamic inactivation of those pathogens *in vitro*, its *in vivo* implementation faces some challenges due to the complexity of the alveolar microenvironment and components such as lung surfactant (LS), an intricate mixture of phospholipids and proteins produced by type II alveolar pneumocytes, covering the entire alveolar surface [19]. Its main functions are to reduce surface tension, prevent the collapse of the alveoli during exhalation, and act as a protective barrier against contaminants that may enter the alveoli environment [20,21]. Recent discoveries from our group have shown the lower efficiency of aPDT in presence of LS is due to the high affinity of PSs for the polar heads of phospholipids. Such a strong interaction has been demonstrated through molecular dynamics simulations, which have indicated LS traps PSs, limiting its binding to the bacterial wall. *In vitro* studies have shown a low concentration of clinical lung surfactant Survanta® is sufficient to inhibit the antimicrobial activity of aPDT *in vitro* with the use of several PSs such as indocyanine green, photoditazine, bacteriochlorin-trizma, and protoporphyrin IX [22]. The only photosensitizer that maintained its action was methylene blue (MB) – however, its absorption at ~670 nm limits the light penetration into the tissue [23]. The pathology and infectious nature of pneumonia require a search for the least invasive treatment, and the use of external infrared lighting appears to be the most suitable.

Recognizing pneumonia as one of the most significant global public health challenges and given the urgent need for new treatments that are effective against a broad range of microorganisms and do not contribute to resistance, this study investigated several physicochemical approaches (*e.g.*, use of perfluorocarbon compounds, association of ICG with oxygen nanobubbles, emulsifiers, and copolymers) towards improving the aPDT response by facilitating permeation through the lung surfactant barrier. The entire path to the most promising solution is discussed and explored in this paper.

2. Materials and methods

2.1. Photosensitizer, lung surfactant, and light source

Indocyanine green 1.3 mM (Ophtalmos, São Paulo, Brazil) was prepared in sterile water on the same day of each experiment and lung surfactants Survanta® (AbbVie, North Chicago, USA) and Curosurf® (Chiesi, Parma, Italy) were used at a final concentration of 5 % (v/v), at which the photodynamic action of several photosensitizers is inhibited [24]. A stock solution was prepared for the tests with dipalmitoylphosphatidylcholine (DPPC) (Lipid Ingredients, Ribeirão Preto, Brazil) considering its concentration in Survanta® (11–15.5 mg/mL) [25] for achieving a final concentration of 0.1 to 20 % (v/v). Illumination was performed after the photosensitizer incubation (from 0 to 40 min) by a LED-based system with emission at 808 nm and 60 mW/cm^2 irradiance (figure S1). The delivered fluence was 20 or 40 J/cm^2.

2.2. ICG combined with emulsifiers and perfluorooctyl bromide

Emulsifiers Pluronic® F-127 (Sigma Aldrich, Saint Louis, USA), Tween® 80 (Êxodo Científica, Sumaré, Brazil), Sodium Dodecyl Sulfate (SDS) (Acros Organics, Geel, Belgium), and Sodium Cholate (Sigma Aldrich, Saint Louis, USA) were added to the experimental medium containing LS and bacteria 30 min prior to the addition of ICG at 0.01 to 1 % final concentrations.

Formulations with perfluorooctyl bromide (PFOB) (Oakwood Chemical, Estill, USA) were prepared with Pluronic® F-127 and Tween® 80. The masses or volumes of those emulsifiers were aliquoted according to the working concentrations (0.03, 0.05, and 0.07 % (w/v) for Pluronic and 0.1, 0.5, and 1 % (v/v) for Tween) and PFOB was added (70 % (v/v)). The sample was vortexed and the ICG solution was then added and stirred again. The formulations were used immediately.

2.3. ICG associated with oxygen nanobubbles

The association of ICG with oxygen nanobubbles (ICG-NBs-O_2) followed the methods described by Yang *et al.* [26]. A hermetically sealed vial was filled with 2 mL of water and saturated with oxygen, ensuring an oxygen-rich atmosphere for the obtaining of free oxygen nanobubbles. Subsequently, a medical syringe containing 3 mL of oxygen was connected to the vial and oxygen nanobubbles were formed through periodic adjustments in the internal pressure, promoting the creation and stabilization of the structures. The ICG solution was carefully added to the system containing those nanobubbles. The process triggered the self-assembly of ICG-NBs-O_2, effectively facilitating the incorporation of ICG into the oxygen nanobubbles, as described in the literature.

2.4. ICG and PVM/MA formulations

Polyvinyl Methyl Ether/Maleic Anhydride copolymer (PVM/MA) powder (Gantrez^{TM} AN-139, Ashland, Wilmington, USA) was diluted in Milli-Q water (at 30 % (w/v) concentration), vigorously mixed and heated in an oven at 95°C for the gel formation through hydrolysis of the anhydride groups of the polymer into carboxylic acids. 3, 4, and 5 % (w/v) solutions were then prepared by diluting the stock solution with Milli-Q water. ICG solution (155 uL, 1.3 mM) or Mili-Q water (for tests using only the polymer) was added, totaling 1 mL of formulation volume. The samples were centrifuged at 3500 rpm for 10 min to ensure complete homogenization and bubble removal. The final polymer concentrations

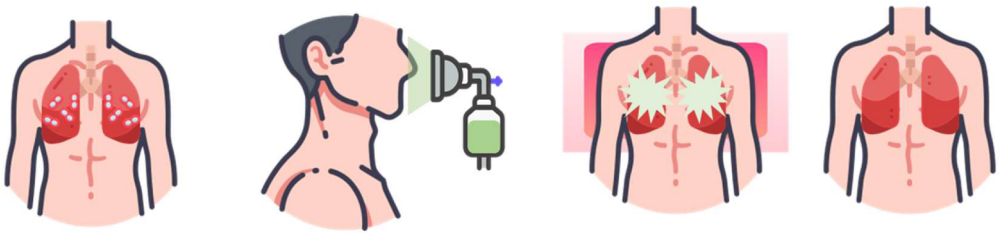

Fig. 1. Schematic representation of the proposed procedure for treating pneumonia through photodynamic action. First, the patient is diagnosed with pneumonia and then a photosensitizer is administered through nebulization. The patient is subsequently exposed to external near-infrared irradiation that activates those molecules in the lungs, reducing the infection load. (Figure created by www.freepik.com).

in the experiments varied between 0.15 and 0.25 % (w/v) and the ICG concentration was set at 10 μM. In addition to the tests employing ICG and PVM/MA in formulation, these components were studied separately – the polymer was added to the medium containing the bacteria and LS 10 60 min before the addition of ICG, followed by 20 min of incubation and subsequent irradiation.

2.5. Bacterial inactivation assays

The experiments were conducted with *Streptococcus pneumoniae* strain (ATCC® 49619™). The bacteria were incubated in Brain Heart Infusion (BHI) at 37 °C, 5 % CO_2, for 4 to 5 h to reach the log phase. The inoculum concentration was then adjusted to approximately 5×10^7 CFU/mL and distributed in 96-well plates (2.5×10^6 CFU/well). The formulations with ICG or free ICG and Curosurf®/Survanta® (in specific groups) were added, reaching the final concentrations of 10 μM and 5 % (v/v), respectively. The samples were incubated at 37 °C in the dark for 0 to 40 min and subsequently irradiated, serially diluted, cultured on blood agar, and incubated at 37 °C for approximately 18 to 24 h for colony counting. Preliminary experiments were conducted on one occasion in triplicate (n = 3) and the remaining ones (with PVM/MA) were carried out on three separate occasions in triplicate (n = 9).

2.6. Measurements of optical properties and zeta potential

The absorption spectra of the formulations and ICG or free polymer were obtained at concentrations of 0.15, 0.2, and 0.25 % (w/v), combined or not with 5 % (v/v) of Survanta®, and the absorbance spectra (Cary 50 Varian Bio UV Vis, Agilent, Santa Clara, USA) were acquired at room temperature in the 300–1000 nm range. 780 nm $\lambda_{excitation}$ and 800–1000 nm $\lambda_{detection}$ were used for the fluorescence spectrum (Cary Eclipse Fluorescence Spectrophotometer, Agilent, Santa Clara, USA).

The zeta potential was measured by Dynamic Light Scattering (DLS) technique, via Zetasizer Lab (Malvern Panalytical). The concentrated samples were diluted (1:20) in Milli-Q water and readings were performed in triplicate.

2.7. Cytotoxicity assay

The *in vitro* experiments were conducted in human lung epithelial cells A549 (ATCC® CCL-185™) and lung fibroblast cells MRC-9 (ATCC® CCL-212™) related to (1) production of lung surfactant and (2) repair of damaged tissue and modulation of the immune response, respectively [27,28]. A549 human cells were cultured in Ham's F-12K medium (Kaighn's) and MRC-9 were cultured in EMEM (Eagle's Minimum Essential Medium), both of them supplemented with 10 % fetal bovine serum (FBS). In a 96-well plate, 10^4 cells were plated in each well and incubated at 37°C, 5 % CO2 for 18–24 h for each experiment.

The culture medium was then removed and the cells were incubated with PVM/MA solutions (preparation with F-12K or EMEM medium described in item 2.4) at 0.15, 0.2, and 0.25 (w/v) concentrations, *i.e.*, the same used in microbiological assays, for 40 min in an incubator. The polymer solution was removed from the wells and washed with PBS. A viability assay was then carried out with 3-[4,5-dimethyl-thiazol-2-yl]-2,5-diphenyltetrazolium bromide (MTT, Sigma Aldrich, Saint Louis, USA).

The samples were incubated for 3 h with MTT, the reagent was removed, and formazan crystals were dissolved in 100 μL of DMSO in each well. Thermo Scientific™ Multiskan™ (Waltham, USA) (for A549) and Infinite® M Nano Tecan (Männedorf, Switzerland) (for MRC-9) plate readers measured absorbance at 570 and 690 nm wavelengths. Absorption at 570 nm was subtracted from absorption at 690 nm (background), then normalized by absorption of the control condition (untreated cells). The experiments were conducted on three separate occasions, in sextuplicate (n = 18).

2.8. Data processing and statistical analysis

All data were processed by Origin 2022b. The statistical analysis was performed with one-way ANOVA (Analysis of Variance) and Tukey's post-hoc at 5 % significance level ($p < 0.05$) for experiments with $n \geq 9$. A smoothing processing by Savitzky–Golay method was applied to absorbance and fluorescence data for reducing noise.

3. Results and discussion

3.1. Use of emulsifiers and formulations with PFOB

Kassab *et al.* [22] reported aPDT mediated by different photosensitizers was inhibited by the presence of lung surfactant. According to molecular dynamics simulations, dipalmitoylphosphatidylcholine (DPPC), the most abundant phospholipid of the surfactant, is the main responsible agent for trapping ICG, preventing this PS from reaching the bacterial target. Therefore, an *in vitro* study conducted by our group evaluated the effect of DPPC concentration on the aPDT response (Fig. 2), observing a marked effect on the bacteria inactivation, ranging from 5 $\log_{10}$ reduction (ICG only group) to no reduction when 20 % of phospholipid were applied. Since a 20 % concentration corresponds to 2.65 mg/mL of phospholipids, which is significantly lower than the concentration observed in the alveoli of adult mammals (~50 mg/mL) [29], the alveolar microenvironment certainly limits the aPDT response.

Emulsifiers of different natures - Pluronic F-127 and Tween (non-ionic), SDS and sodium cholate (ionic) were used for permeabilizing the phospholipid organization of LS and enhancing ICG diffusion [30,31]. Such compounds are reported to disaggregate photosensitizers and increase their internalization by microorganisms, thus improving aPDT [32,33]. However, the results in Fig. 3 show none of the concentrations studied promoted microbial reduction in aPDT groups and SDS and sodium cholate are toxic in the dark (0 J/cm^2) starting at 0.1 and 1 % (w/v), respectively.

Another approach investigated consisted of the use of perfluorocarbons (PFC), such as perfluorooctyl bromide (PFOB), which has high solubility of oxygen (an advantageous characteristic for PDT) and carbon dioxide, high spreading coefficient, low surface tension and viscosity, which enables its flowing through extremely narrow airways [34,35]. Previous studies with vasoactive drugs [36], antibiotics [37,38], and plasmids [39,40] have reported PFCs are effective vehicles for drug delivery throughout the lung. However, those compounds have hydro-lipophobic characteristics, which make them quite immiscible

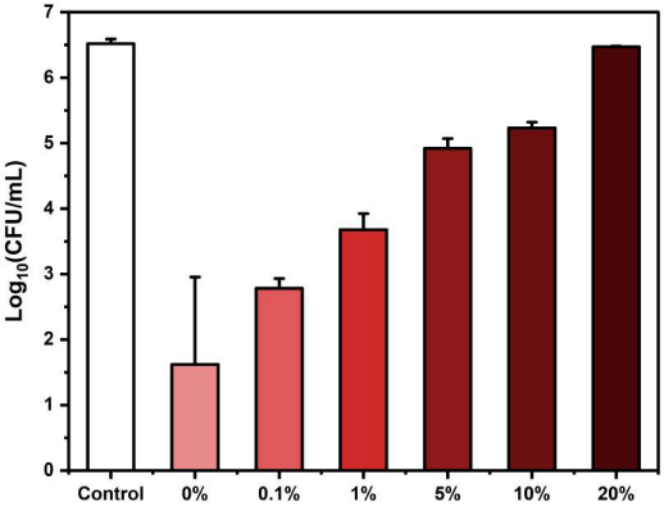

Fig. 2. Influence of dipalmitoylphosphatidylcholine (DPPC) concentration on the photodynamic inactivation of *S. pneumoniae* with the use of ICG (10 μM) (20 J/cm^2, 20 min incubation) (n = 3).

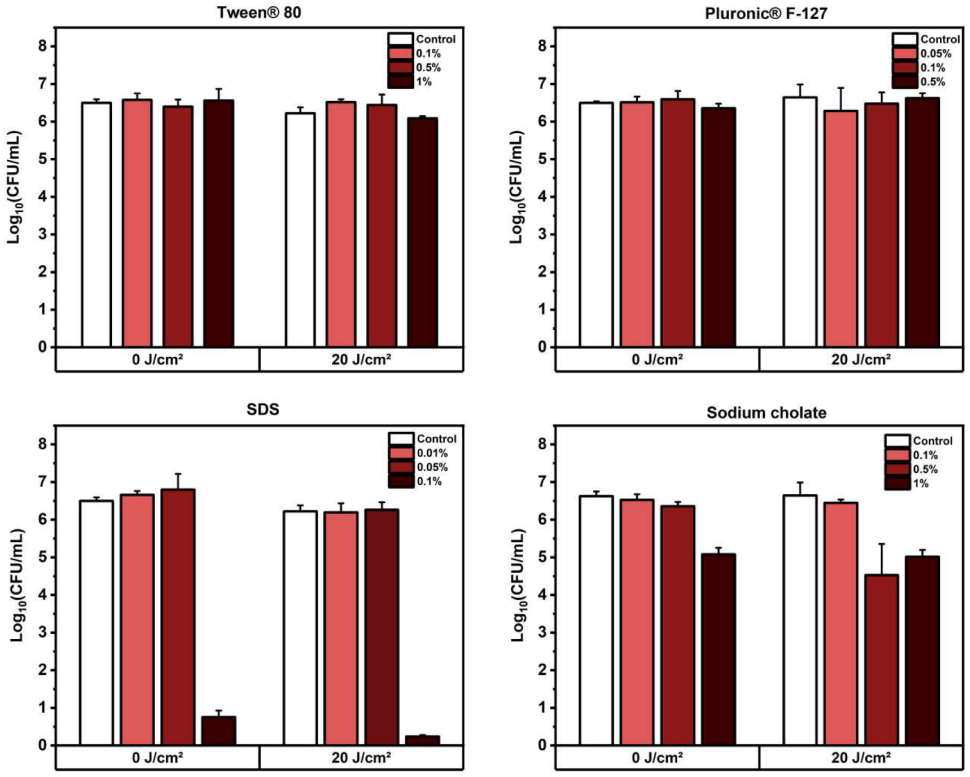

Fig. 3. Inactivation of *S. pneumoniae* using ICG (10 μM) in a medium containing emulsifiers at different concentrations and 5 % (v/v) Curosurf® (20 min incubation) (n = 3).

and require the use of emulsifiers for obtaining formulations. Tween® 80 and Pluronic® F-127 were used in different concentrations, with 70 % (v/v) of PFOB. The results are shown in Fig. 4.

Several studies have demonstrated the use of PFCs in aPDT is very promising, mainly due to their intrinsic oxygen transport capacity [41–43]. However, under the conditions adopted here, such capacity was not considerable to promote desirable antimicrobial responses and, due to its inert nature, PFOB may have neither interacted sufficiently with ICG, nor provided it with mobility, leaving the molecule free to be captured by LS.

3.2. Use of oxygen nanobubbles

An alternative that emerged was the association of ICG with oxygen nanobubbles (ICG-NBs-O_2), considered interesting for increasing quantum yield in the production of singlet oxygen of photosensitizers [26]. Therefore, with the use of that composition, it was believed that, even with the limitation of molecular mobility, the few ICG molecules that reached the bacterial colonies would be sufficient to inactivate them, given the increase in the production of ROS. Fig. 5 shows the results - although significant, a 2 $\log_{10}$ reduction is below the one desired for the treatment of the infection, according to the American Society of Microbiology, which states any new approach must promote a 99.9 % reduction in microbial load (or at least 3 $\log_{10}$) [44] to be considered antimicrobial.

Studies that used oxygen nanobubbles employed mainly perfluorocarbons in their composition, since they are excellent carriers of that gas. The simple association of PS with nanobubbles was reported only by Yang *et al.* [26], who used them with ICG to overcome tumor hypoxia, with great success in the treatment of oral cancer in an animal model using PDT.

Therefore, the significant challenge posed by LS becomes evident,

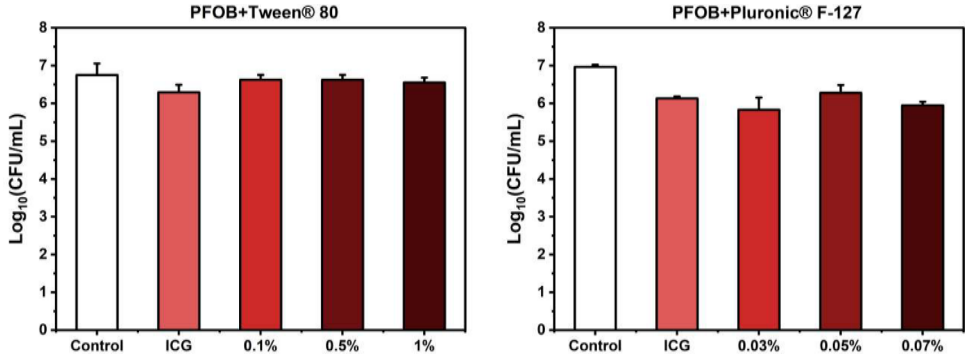

Fig. 4. Photodynamic inactivation of *S. pneumoniae* using formulations of ICG (10 μM) + PFOB (70 % (v/v)) combined with different concentrations of emulsifiers (0.1 to 1 % (v/v) Tween 80 and 0.03 to 0.07 % (w/v) Pluronic F-127) in a medium containing 5 % (v/v) of Curosurf® (20 J/cm^2, 20 min incubation). The ICG group refers to the use of pure PS (n = 3).

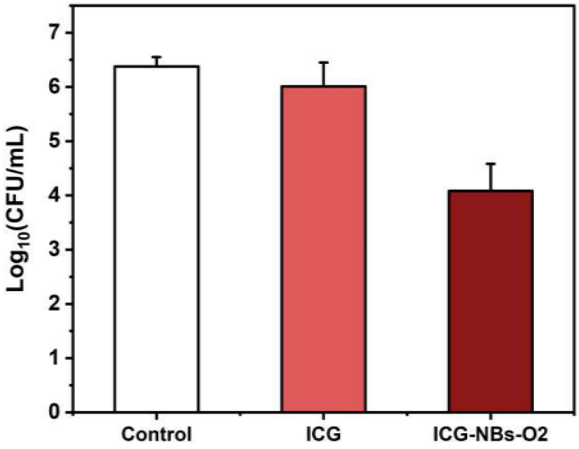

Fig. 5. Photodynamic inactivation of *S. pneumoniae* using ICG-NBs-O_2 (10 μM) in a medium containing 5 % (v/v) Curosurf® (20 J/cm^2, 20 min incubation) (n = 3).

since several promising strategies for optimizing PDT for different applications have proven ineffective in promoting considerable antimicrobial responses in an alveolar environment containing LS.

3.3. Combination of ICG with copolymers - a promising alternative for successful lung aPDT

PVM/MA has been considered a versatile drug carrier with various applications (*e.g.*, production of dissolvable microneedles for skin cancer treatment using PDT, as reported by our team [45]). Such copolymers (PVM/MA) are biodegradable molecules of low toxicity, high biocompatibility and mucoadhesiveness, and low cost [46,47] and have been widely used in food, pharmaceutical, and oral care industries [48–50].

Since a small or no microbial reduction was observed in the approaches studied, the incubation time and fluence adopted in the initial tests with PVM/MA were 40 min and 40 J/cm^2, respectively, for maximizing the interaction between the photosensitizer and the bacteria and the treatment response (Fig. 6) [51,52]. The combination of 0.2 % (w/v) of the polymer with ICG eradicated the microbial load - at this concentration, the polymer alone is not toxic either in the dark, or when irradiated (Figure 6(a)). On the other hand, at 0.25 % (w/v), it is bactericidal (Figure 6(b) and (c)), indicating the 0.2 % (w/v) concentration is the ideal one due to the bacterial death only in the aPDT group. The narrow window of copolymer concentration possibilities between a complete phototoxicity action of PVM/MA-ICG in relation to PVM/MA seemed to be a limiting factor at first in this proof of principle. However, in an *in vivo* situation, such a condition must be severely expanded in function of the great responsiveness of the system as a whole. In fact, preliminary animal experiments indicated a much broader window in that regard (data not shown), which will be explored in future research, with detailed reports of *in vivo* experiments

Additional tests with a 0.2 % (w/v) concentration checked whether the same photoinactivation profile was observed with drug-light intervals shorter than 40 min and with the standard light dose used in previous studies (20 J/cm^2) for optimizing the photoinactivation protocol. An optimized photodynamic inactivation protocol (phototoxic to bacteria with minimum damage to the host) includes a 5 to 10 min incubation period and an at least 3 $\log_{10}$ reduction in microbial load [44]. The data in Fig. 7 show after 10 min, the reduction in microbial load is complete; therefore, a 40-min incubation, as initially applied, is not necessary, indicating ICG associated with the copolymer shows great potential for lung decontamination.

In view of *in vivo* experiments, the efficiency of the administration of the polymer prior to ICG for microbial inactivation and the relation of the mechanism involved to the association of the polymer with LS for leaving ICG free must be checked. The results in Fig. 8 show the introduction of the polymer prior to ICG is not effective for bacterial reduction, indicating a previous connection between the two components is essential for the success of the therapy. The presence of highly reactive anhydride residues in the polymer provides this component with the ability to bind to different nucleophiles. Therefore, PVM/MA must

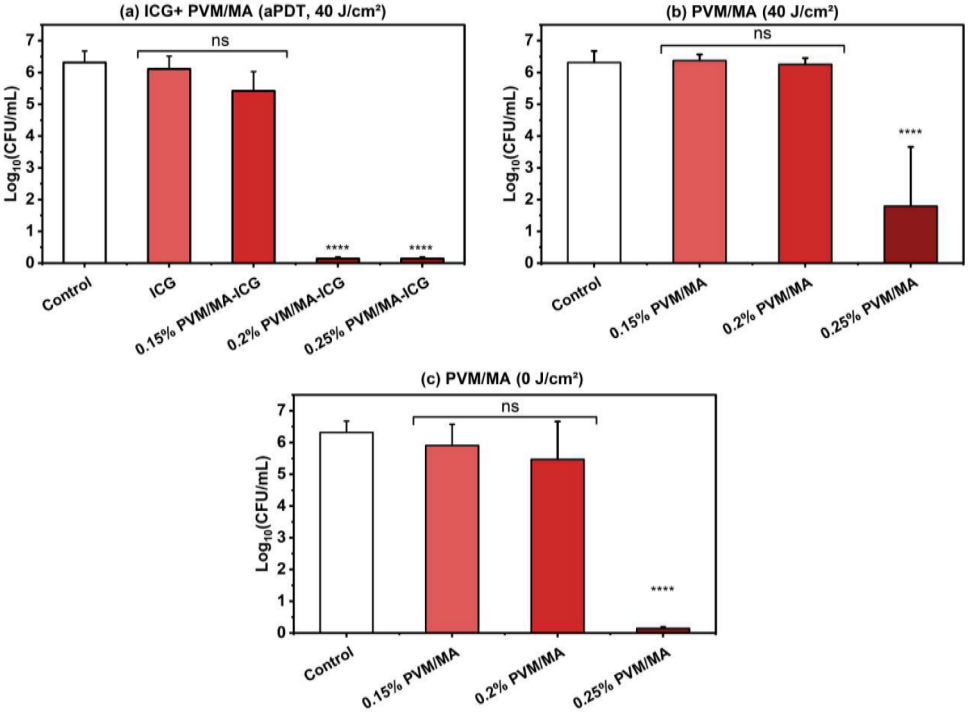

Fig. 6. Antimicrobial effect of PVM/MA according to its concentration %(w/v) in a medium containing 5 % (v/v) of Curosurf®: (a) combined with ICG (10 μM) (aPDT, 40 J/cm^2, 40 min incubation); (b) irradiated (40 J/cm^2), and (c) in the dark (0 J/cm^2) (n = 9). ns: not significant ($p > 0.05$); ****$p < 0.0001$.

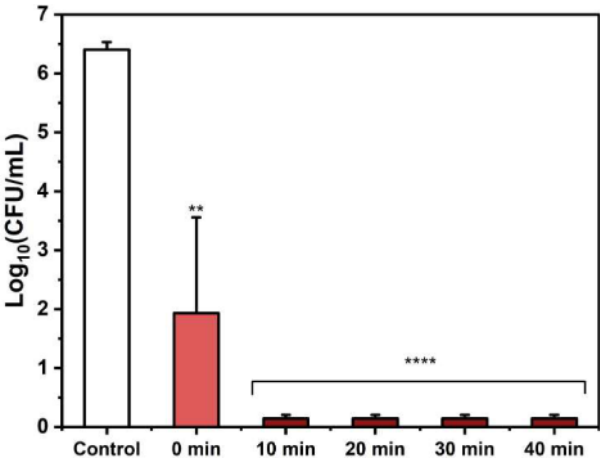

Fig. 7-. Influence of incubation time on the photodynamic inactivation of *S. pneumoniae* with the use of 0.2 (w/v) PVM/MA + 10 μM ICG and 20 J/cm^2 in a medium containing 5 % (v/v) of Survanta® (n = 9); $^{**}p < 0.01$; $^{****}p < 0.0001$.

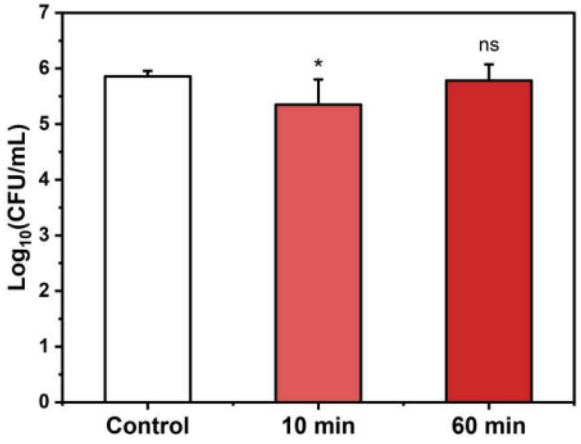

Fig. 8. Effect of addition of PVM/MA (0.2 % (w/v)) prior to the addition of ICG (10 μM) at 10 and 60 min intervals on aPDT, in a medium containing 5 % (v/v) of Survanta® (20 J /cm^2, 20 min incubation) (n = 6); ns: not significant ($p > 0.05$); $^{*}p \leq 0.05$.

develop a sufficiently strong interaction with ICG, protecting the PS cargo and preventing it from associating with the phospholipids of the lung surfactant, thus being available for interaction with the bacteria and inactivating them after irradiation [53,54].

Absorption and fluorescence spectra of free ICG and formulations were obtained for a better understanding of that interaction. ICG in ionized solutions, such as PBS, is known to have a high probability of forming aggregates. The free ICG spectrum shows a monomeric peak centered at 780 nm and an H-aggregate peak at 705 nm. When ICG was associated with PVM/MA, its spectroscopic properties changed, indicating a connection between the photosensitizer and the polymer, with a reduction and a broadening of the absorption peaks with a red shift (Fig. 9). Such characteristics reveal ICG may be largely associated with the polymer in its aggregated form in that buffer. The same spectral behavior was observed by Kumari and collaborators [55,56] when encapsulating ICG with poly-l-arginine and poly-l-lysine. They corroborated the hypothesis by collecting fluorescence emission spectra, when a decrease in intensity in relation to free ICG could be attributed to quenching caused by aggregation. The fluorescence emission spectra of free ICG and formulations with PVM/MA are shown in Fig. 10, where a reduction in the fluorescence emission of ICG when combined with the polymer can be observed.

Regarding analyses in PBS with 5 % Survanta®, a strong decrease in aggregation occurred from the absorbance spectrum, with a prevalence of monomers (Fig. 9), whereas the difference in fluorescence between the formulation and free ICG is significantly smaller compared to the spectrum obtained in PBS alone, with a red shift also occurring (Fig. 10).

Both absorption and fluorescence intensity decreased in all spectra (with or without Survanta®) as the concentration of PVM/MA increased in the formulation – that was another indication of the polymer influence on ICG aggregation. The zeta potential (ZP) values (Table 1) also support the hypothesis, since the values obtained for the formulation and for the polymer in modulus were lower than those for free ICG. Zeta potential is directly related to the stability of the solution, where typically, the most favorable values are above 30 mV in magnitude, since, under these conditions, particles repel each other and resist aggregate formation [57]. Interestingly, such effects were not detrimental to the photodynamic action, as demonstrated elsewhere, with excellent microbial reduction in presence of LS.

The polymer is believed to produce a type of photosensitizer folding, providing a shield to the molecules, which now have mobility through the surfactant. The unfolding of the polymer placing ICG molecules in contact with the environment occurs after a wide distribution throughout the system and in the vicinity of bacterial colonies. Therefore, due to the importance of the complexation between PS and the polymer for the success of aPDT, both integrity and disposition of those molecules after the nebulization process (the intended route of administration) must be investigated. Challenges in function of the considerable viscosity of the formulation as the polymer concentration increases are expected.

3.4. Cytotoxicity assays of PVM/MA

The toxicity of PVM/MA in health mammalian cells was measured in lung epithelial (A549) and fibroblast (MRC-9) cell lines. MTT assays were first conducted with the most promising concentration for

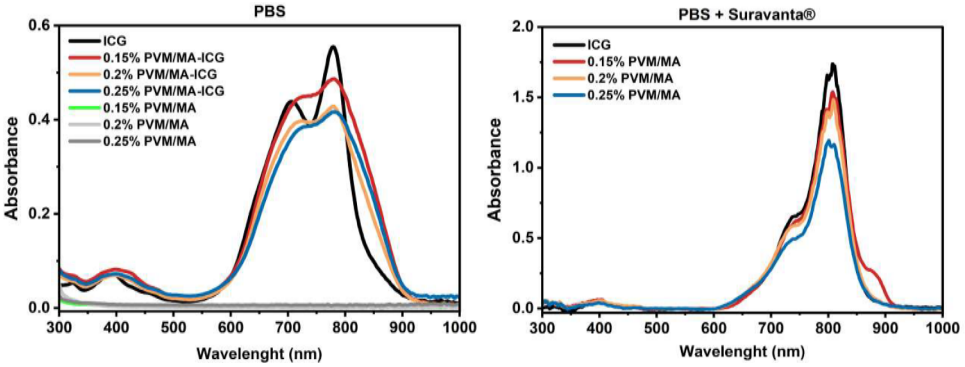

Fig. 9. Absorption spectra of both formulation and ICG and free polymer in PBS with or without 5 % Survanta®.

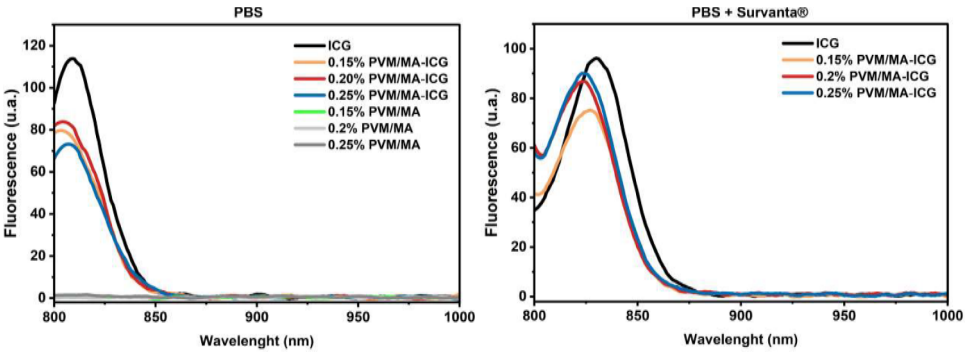

Fig. 10. Fluroescence spectra of both formulation and ICG and free polymer in PBS with or without 5 % Survanta®.

Table 1
Zeta potential of the polymer, free ICV, and formulation.

Sample	Zeta potential (mV)
0.2 % (w/v) PVM/MA	-5.2 ± 0.2
10 μM ICG	-23.8 ± 4.3
0.2 % (w/v) PVM/MA - 10 μM ICG	- 20.8 ± 1.3

microbial inactivation (0.2 % (w/v) or 2 mg/mL), which, according to Fig. 11, does not cause cytotoxicity to the cell lines studied.

Souza *et al.*, [58] observed no reduction in A549 viability for discharged PVM/MA nanoparticles (polymer only) at 150 μg/mL concentration even after 72 h incubation. Similar results in Caco2 cell line incubated for up to 72 h with PVM/MA nanoparticles at 2 mg/mL concentration were reported by Ojer *et al.* [59]. On the other hand, toxicity showed to be time-dependent for HepG2 – no reduction in cell viability with up to 48 h incubation was observed for 1 mg/mL; however, above 72 h, viability showed an around 80 % reduction. Muehlmann *et al.* [60] assessed a higher concentration (7.2 mg/mL), but with shorter incubation time (15 minutes) and reported no reduction in the viability of 4T1, NIH/3T3, MCF-7, and MCF-10A cell lines.

The results show the importance of evaluating cytotoxicity at different concentrations and incubation times – such parameters will be the target of subsequent studies involved in this research.

Although some studies still must be conducted for complementing the understanding of those copolymers in lung tissues, advancements have been made towards overcoming LS and enabling pulmonary aPDT with the use of ICG, a PS well established and studied, and PVM/MA, a highly biocompatible polymer.

4. Conclusions

According to the results, the use of perfluorocarbons, emulsifiers, and oxygen nanobubbles is not effective for overcoming the lung surfactant barrier for the success of aPDT. However, the combination of 10 μM of ICG with 0.2 % (w/v) of PVM/MA—a polymer that has proven highly effective for PS delivery—led to the eradication of the microbial load of *S. pneumoniae*. Spectroscopic analyses revealed the complexation of those components, with spectral band broadening and decreased fluorescence of PS compared to its free form. Regarding the toxicity of PVM/MA for human lung cells, MTT assays showed no reduction in cell viability, indicating high biocompatibility of the polymer. The results indicate the potential of PVM/MA as a drug delivery vehicle to the lungs, enabling the transposition of the lung surfactant, and a promising solution for the success of aPDT in the treatment of pneumonia. The next steps in this research will focus on transferring the inactivation protocol proposed to an animal model.

CRediT authorship contribution statement

Isabelle Almeida de Lima: Writing – original draft, Visualization, Methodology, Investigation, Formal analysis, Data curation, Conceptualization. **Lorraine Gabriele Fiuza:** Writing – review & editing, Investigation. **Johan Sebastián Díaz Tovar:** Writing – review & editing, Investigation. **Dianeth Sara Lima Bejar:** Writing – review & editing, Investigation. **Ana Julia Barbosa Tomé:** Writing – review & editing, Investigation. **Michelle Barreto Requena:** Writing – review & editing, Investigation. **Layla Pires:** Writing – review & editing, Investigation. **Gang Zheng:** Writing – review & editing. **Natalia Mayumi Inada:** Writing – review & editing, Validation, Project administration, Methodology, Conceptualization. **Cristina Kurachi:** Writing – review & editing, Validation, Project administration, Methodology, Conceptualization. **Vanderlei Salvador Bagnato:** Writing – original draft, Validation, Supervision, Methodology, Funding acquisition, Conceptualization.

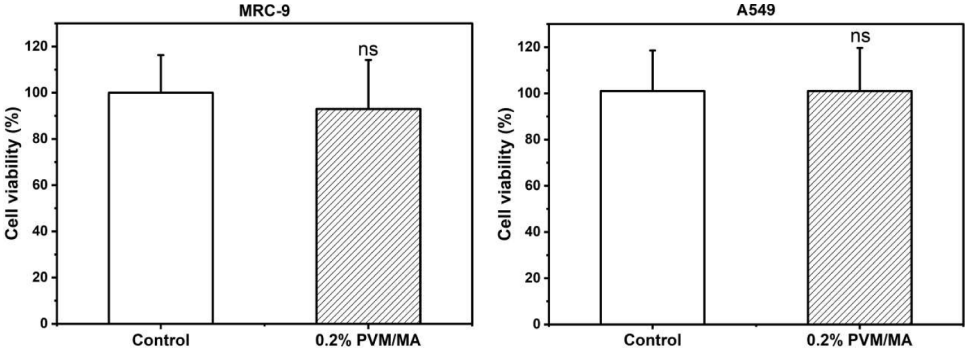

Fig. 11. Cell viability of MRC-9 and A549 lines after incubation for 40 min with 0.2 % (w/v) PVM/MA. MTT assay was performed immediately after incubation. Results presented in % in relation to the control (n = 18). ns: not significant ($p > 0.05$).

Declaration of competing interest

The authors declare that they have no known competing financial interests or personal relationships that could have appeared to influence the work reported in this paper.

Data availability

All the study data are included in the article and the supplementary material.

Acknowledgments

The authors acknowledge the strong international collaboration and the financial support provided by FAPESP (grants 2013/07276-1, 2022/03965-6, 2022/10860-6 and 2023/04209-3) and CNPq (grant 465360/2014-9) Brazilian agencies, as well as CPRIT (grant M20301556), GURI (grant M230930) and CRI (grant 02-292034) United States of America agencies in Texas. They are also indebted to the Canadian Institute for Health Research (grants FDN154326 and PJT190047).

Supplementary materials

Supplementary material associated with this article can be found, in the online version, at doi:10.1016/j.jpap.2024.100252.

References

[1] N. Ablakimova, L.A. Woodcock, J.S. Fan, M. Si, R. Zhou, R.E.W. Hancock, R. J. Evans, Bibliometric analysis of global research output on antimicrobial resistance among pneumonia pathogens (2013–2023), Antibiotics 12 (2023) (1411), https://doi.org/10.3390/antibiotics12091411.

[2] B. Dadonaite, M. Roser, Pneumonia, Our World Data (2024). Accessed: Aug. 12, 2024. [Online]. Available: https://ourworldindata.org/pneumonia.

[3] J. Tang, Y. Wu, J. Wu, X. Chen, G. Yin, S. Zhao, Nanomaterials for delivering antibiotics in the therapy of pneumonia, Int. J. Mol. Sci. 23 (2022) 15738, https://doi.org/10.3390/ijms232415738.

[4] C. Cillóniz, C. Dominedò, A. Torres, Multidrug resistant gram-negative bacteria in community-acquired pneumonia, Crit. Care 23 (2019) 1–9, https://doi.org/10.1186/s13054-019-2371-3.

[5] S. Kwiatkowski, A. Knap, M. Przystupski, P. Saczko, J. Kędzierska, K. Knap-Czop, J. Kotlińska, L. Michel, J. Kotowski, J. Kulbacka, Photodynamic therapy – mechanisms, photosensitizers and combinations, Biomed. Pharmacother. 106 (2018) 1098–1107, https://doi.org/10.1016/j.biopha.2018.07.049.

[6] F. Cieplik, A. Tabenski, C. Buchalla, A. Al-Ahmad, Antimicrobial photodynamic therapy – what we know and what we don't, Crit. Rev. Microbiol. 44 (2018) 571–589, https://doi.org/10.1080/1040841x.2018.1467876.

[7] Y. Liu, R. Qin, S.A.J. Zaat, E. Breukink, M. Heger, R. van Golen, Antibacterial photodynamic therapy: overview of a promising approach to fight antibiotic-resistant bacterial infections, J. Clin. Transl. Res. 1 (2015) 140–167, https://doi.org/10.18053/jctres.201503.002.

[8] Y. Jao, S.J. Ding, C.C. Chen, Antimicrobial photodynamic therapy for the treatment of oral infections: a systematic review, J. Dent. Sci. 18 (2023) 1453–1466, https://doi.org/10.1016/j.jds.2023.07.002.

[9] J.A. Willis, H. Cui, J. Li, J.R. Tumilty, B.U. Jain, M.S. Nam, A. Lim, N.J. Chew, A. K. Pearce, S.P. Armes, C.K. Weiss, Breaking down antibiotic resistance in methicillin-resistant *Staphylococcus aureus*: Combining antimicrobial photodynamic and antibiotic treatments, Proc. Natl. Acad. Sci. U. S. A. 119 (2022) e2208378119, https://doi.org/10.1073/pnas.2208378119.

[10] J.M. Soares, V.V. Yakovlev, K.C. Blanco, V.S. Bagnato, Recovering the susceptibility of antibiotic-resistant bacteria using photooxidative damage, Proc. Natl. Acad. Sci. U. S. A. 120 (2023), https://doi.org/10.1073/pnas.2311667120 e2311667120.

[11] I.S. Leite, K.C. Blanco, N.M. Inada, E. Bagnato, V.S. Bagnato, Near–infrared photodynamic inactivation of *S.* pneumoniae and its interaction with RAW 264.7 macrophages, J. Biophotonics 11 (2018) e201600283, https://doi.org/10.1002/jbio.201600283.

[12] G. Kassab, M.C. Geralde, N.M. Inada, A.E. Achiles, V.G. Guerra, V.S. Bagnato, Nebulization as a tool for photosensitizer delivery to the respiratory tract, J. Biophotonics 12 (2019) e201800189, https://doi.org/10.1002/jbio.201800189.

[13] J.S. Díaz Tovar, G. Kassab, H.H. Buzzá, V.S. Bagnato, C. Kurachi, Photodynamic inactivation of *Streptococcus pneumoniae* with external illumination at 808 nm through the ex vivo porcine thoracic cage, J. Biophotonics 15 (2022) e202100189, https://doi.org/10.1002/jbio.202100189.

[14] C. Pérez, T. Zúñiga, C.E. Palavecino, Photodynamic therapy for treatment of *Staphylococcus aureus* infections, Photodiagnosis Photodyn. Ther. 34 (2021) 102285, https://doi.org/10.1016/j.pdpdt.2021.102285.

[15] T.W. Wong, M.H. Sung, K.C. Chen, Indocyanine green—mediated Photodynamic Therapy reduces methicillin-resistant *Staphylococcus aureus* drug resistance, J. Clin. Med. 8 (2019) 411, https://doi.org/10.3390/jcm8030411.

[16] M. Miyabe, J.C. Junqueira, A.C.B. Pereira, A.O.C. Jorge, M.S. Ribeiro, I.S. Feist, A. C.B. Pereira, Effect of photodynamic therapy on clinical isolates of *Staphylococcus* spp, Braz. Oral Res. 25 (2011) 230–234, https://doi.org/10.1590/S1806-83242011005000006.

[17] M. Valenzuela-Valderrama, I.A. González, C.E. Palavecino, Photodynamic treatment for multidrug-resistant Gram-negative bacteria: perspectives for the treatment of *Klebsiella pneumoniae* infections, Photodiagnosis Photodyn. Ther. 28 (2019) 256–264, https://doi.org/10.1016/j.pdpdt.2019.08.012.

[18] Y. Xie, J. Jiang, X. Fu, Y. Wang, T. Chen, X. Xu, J. Yuan, C. Yang, Z. Luo, Antimicrobial efficacy of aloe-emodin mediated photodynamic therapy against antibiotic-resistant *Pseudomonas aeruginosa in vitro*, Biochem. Biophys. Res. Commun. 690 (2024) 149285, https://doi.org/10.1016/j.bbrc.2023.149285.

[19] Y.Y. Zuo, R.A.W. Veldhuizen, A.W. Neumann, N.O. Petersen, F. Possmayer, Current perspectives in pulmonary surfactant — inhibition, enhancement and evaluation, Biochim. Biophys. Acta Biomembr. 1778 (2008) 1947–1977, https://doi.org/10.1016/j.bbamem.2008.03.021.

[20] A. Hidalgo, J.D. Arroyo, J.A. García-Martínez, M.L. Mato, C.G. Gallardo, R.H. Gil, L.R. Pérez-Gil, Pulmonary surfactant and drug delivery: vehiculization, release and targeting of surfactant/tacrolimus formulations, J. Control. Release 329 (2021) 205–222, https://doi.org/10.1016/j.jconrel.2020.11.042.

[21] M. Confalonieri, F. Salton, B. Ruaro, P. Confalonieri, M.C. Volpe, Alveolar epithelial type II cells, Encycl. Respir. Med. 1 (2022) 10–17, https://doi.org/10.1016/B978-0-08-102723-3.00157-8.

[22] G. Kassab, J.S.D. Tovar, L.M.P. Souza, R.K.M. Costa, R.S.S. Silva, A.S. Pimentel, V. S. Bagnato, Lung surfactant negatively affects the photodynamic inactivation of bacteria—*in vitro* and molecular dynamic simulation analyses, Proc. Natl. Acad. Sci. U. S. A. 119 (2022) e2117629119, https://doi.org/10.1073/pnas.2123564119.

[23] S.L. Jacques, Optical properties of biological tissues: a review, Phys. Med. Biol. 58 (2013) R37, https://doi.org/10.1088/0031-9155/58/11/R37.

[24] J.A. Silverman, L.I. Mortin, A.D.G. VanPraagh, T. Li, J. Alder, Inhibition of daptomycin by pulmonary surfactant: *In vitro* modeling and clinical impact, J. Infect. Dis. 191 (2005) 2149–2152, https://doi.org/10.1086/430352.

[25] S. Pham, T.S. Wiedmann, Note: dissolution of aerosol particles of budesonide in Survanta™, a model lung surfactant, J. Pharm. Sci. 90 (2001) 98–104, https://doi.org/10.1002/1520-6017(200101)90:1<98::aid-jps11>3.0.co;2-5.

[26] L. Yang, B. Huang, S. Hu, Y. An, J. Sheng, Y. Li, Y. Wang, N. Gu, Indocyanine green assembled free oxygen-nanobubbles towards enhanced near-infrared induced photodynamic therapy, Nano Res. 15 (2022) 4285–4293, https://doi.org/10.1007/s12274-022-4085-0.

[27] M. Singal, The effect of particle deposition on immunological response as measured by cytokine production, Compar. Biol. Normal Lung: Second Edition (2015) 601–627, https://doi.org/10.1016/B978-0-12-404577-4.00031-X.

[28] K.J. Cavagnero, R.L. Gallo, Essential immune functions of fibroblasts in innate host defense, Front. Immunol 13 (2022) 1058862, https://doi.org/10.3389/fimmu.2022.1058862/bibtex.

[29] X. Xu, G. Li, Y.Y. Zuo, Constrained drop surfactometry for studying adsorbed pulmonary surfactant at physiologically relevant high concentrations, Am. J. Physiol. Lung Cell Mol. Physiol. 325 (2023) L508–L517, https://doi.org/10.1152/ajplung.00101.2023.

[30] L.M.P. Souza, J.B. Nascimento, A.L. Romeu, E.D. Estrada-López, A.S. Pimentel, Penetration of antimicrobial peptides in a lung surfactant model, Colloids Surf. B Biointerfaces 167 (2018) 345–353, https://doi.org/10.1016/j.colsurfb.2018.04.030.

[31] S. Keller, H. Heerklotz, N. Jahnke, A. Blume, Thermodynamics of lipid membrane solubilization by sodium dodecyl sulfate, Biophys. J. 90 (2006) 4509–4521, https://doi.org/10.1529/biophysj.105.077867.

[32] G.A. Collina, F. Freire, V.S. Barbosa, C.B. Correa, H.R. Nascimento, A.C.R. T. Horliana, D.F.T. Silva, R.A. Prates, C. Pavani, Photodynamic antimicrobial chemotherapy action of phenothiazinium dyes in planktonic *Candida albicans* is increased in sodium dodecyl sulfate, Photodiagnosis Photodyn. Ther. 29 (2020) 101612, https://doi.org/10.1016/j.pdpdt.2019.101612.

[33] A.V. Kustov, M.A. Krestyaninov, s.o. Kruchin, O.V. Shukhto, T.V. Kustova, D. V. Belykh, I.S. Khudyaeva, M.O. Koifman, P.B. Razgovorov, D.B. Berezin, Interaction of cationic chlorin photosensitizers with non-ionic surfactant Tween 80, Mendeleev Commun. 31 (2021) 65–67, https://doi.org/10.1016/j.mencom.2021.01.019.

[34] D. Alapati, T.H. Shaffer, Administration of drugs/gene products to the respiratory system: a historical perspective of the use of inert liquids, Front. Physiol. 13 (2022) 871893, https://doi.org/10.3389/fphys.2022.871893/bibtex.

[35] M. Chenoune, L. Rochefort, P. Bruvenal, F. Lidouren, M. Kohllhauer, A. Seemann, B. Ghaleh, M. Korn, R. Dubuisson, A.B. Yahmed, X. Maître, D. Isabey, J. Ricard, R. E. Kerber, L. Darrasse, A. Berdeaux, R. Tissier, Evaluation of lung recovery after static administration of three different perfluorocarbons in pigs, BMC Pharmacol. Toxicol. 15 (2014) 53, https://doi.org/10.1186/2050-6511-15-53/figures/4.

[36] M.R. Wolfson, J.S. Greenspan, T.H. Shaffer, Pulmonary administration of vasoactive substances by perfluorochemical ventilation, Pediatrics 97 (1996) 449–455, https://doi.org/10.1542/peds.97.4.449.

[37] D.J. Smith, L.M. Gambone, T. Tarara, d.r. Meays, L.A. dellamary, C.M. Woods, J. Weers, Liquid dose pulmonary instillation of gentamicin pulmoSpheres®

formulations: Tissue distribution and pharmacokinetics in rabbits, Pharm. Res. 18 (2001) 1556–1561, https://doi.org/10.1023/a:1013078330485/metrics.
[38] R.A. Orizondo, D.L. Nelson, M.L. Fabiilli, K.E. Cook, Effects of fluorosurfactant structure and concentration on drug availability and biocompatibility in water-in-perfluorocarbon emulsions for pulmonary drug delivery, Colloid Polym. Sci. 295 (2017) 2413. Accessed: Dec. 14, 2023. [Online]. Available: /pmc/articles/pmc6133303/.
[39] D.A. Lisby, P.L. Ballard, W.W. Fox, M.R. Wolfson, T.H. Shaffer, L.W. Gonzales, Enhanced distribution of adenovirus-mediated gene transfer to lung parenchyma by perfluorochemical liquid, Hum. Gene Ther. 8 (2008) 919–928, https://doi.org/10.1089/hum.1997.8.8-919.
[40] D.J. Weiss, T.P. Strandjord, D. Liggitt, J.G. Clark, Perflubron enhances adenovirus-mediated gene expression in lungs of transgenic mice with chronic alveolar filling, Hum. Gene Ther. 10 (2004) 2287–2293, https://doi.org/10.1089/10430349950016933.
[41] P. Niu, J. Dai, Z. Wang, Y. Wang, D. Feng, Y. LI, W. Miao, Sensitization of antibiotic-resistant gram-negative bacteria to photodynamic therapy via perfluorocarbon nanoemulsion, Pharmaceuticals 15 (2022) 156, https://doi.org/10.3390/ph15020156/s1.
[42] M. Wu, C. Chen, Z. Liu, J. Tian, W. Zhang, Regulating the bacterial oxygen microenvironment via a perfluorocarbon-conjugated bacteriochlorin for enhanced photodynamic antibacterial efficacy, Acta Biomater. 142 (2022) 242–252, https://doi.org/10.1016/j.actbio.2022.02.013.
[43] K.H. Hsiao, C.M. Huang, Y.H. Lee, Development of Rifampicin-Indocyanine green-loaded perfluorocarbon nanodroplets for photo-chemo-probiotic antimicrobial therapy, Front. Pharmacol. 9 (2018) 412359, https://doi.org/10.3389/fphar.2018.01254/bibtex.
[44] E. Alves, M.A.F. Faustino, M.G.P.M.S. Neves, A. Cunha, J. Tome, A. Almeida, An insight on bacterial cellular targets of photodynamic inactivation, Future Med. Chem. 6 (2014) 141–164, https://doi.org/10.4155/fmc.13.211.
[45] M.B. Requena, A.D. Permana, J.D. Vollet-Filho, P. González-Vásquez, M.R. Garcia, C.M.G. Faria, S. Pratavieira, R.F. Donnelly, V.S. Bagnato, Dissolving microneedles containing aminolevulinic acid improves protoporphyrin IX distribution, J. Biophotonics 14 (2021), https://doi.org/10.1002/jbio.202000128.e202000128.
[46] A. Mira, C.R. Mateo, R. Mallavia, A. Falco, Poly(methyl vinyl ether-alt-maleic acid) and ethyl monoester as building polymers for drug-loadable electrospun nanofibers, Sci. Rep. 7 (2017) 1–13, https://doi.org/10.1038/s41598-017-17542-4.
[47] T. Iglesias, M. Dusinska, N. El Yamani, J.M. Irache, A. Azqueta, A. López de Cerain, *In vitro* evaluation of the genotoxicity of poly(anhydride) nanoparticles designed for oral drug delivery, Int. J. Pharm. 523 (2017) 418–426, https://doi.org/10.1016/j.ijpharm.2017.03.016.
[48] E. Prieto, C.S. Rodriguez, M. Fernández, A. Merino, R. Jiménez, Gantrez AN nanoparticles for ocular delivery of memantine: *in vitro* release evaluation in albino rabbits, Ophthalmic Res. 48 (2012) 109–117, https://doi.org/10.1159/000337136.
[49] E. Caló, J. Barros, L. Ballamy, V.V. Khutoryanskiy, Poly(vinyl alcohol)–Gantrez® AN cryogels for wound care applications, RSC Adv. 6 (2016) 105487–105494, https://doi.org/10.1039/c6ra24573k.
[50] Scientific opinion on the safety of 'methyl vinyl ether-maleic anhydride copolymer' (chewing gum base ingredient) as a novel food ingredient, EFSA J. 11 (2013) 3423, https://doi.org/10.2903/j.efsa.2013.3423.
[51] Z. Zhao, Y. Zhang, H. Liu, Y. Chen, X. Liu, Antimicrobial photodynamic therapy combined with antibiotic in the treatment of rats with third-degree burns, Front. Microbiol. 12 (2021) 622410, https://doi.org/10.3389/fmicb.2021.622410.
[52] R. Wiench, L. Ramakrishna, E.G.G. Lima, N.B. Torres, J. Silveira, Influence of incubation time on ortho-toluidine blue mediated antimicrobial photodynamic therapy directed against selected *Candida strains*—an *in vitro* study, Int. J. Mol. Sci. 22 (2021) 10971, https://doi.org/10.3390/ijms222010971.
[53] Y.W. Noh, H.S. Park, M.H. Sung, Y.T. Lim, Enhancement of the photostability and retention time of indocyanine green in sentinel lymph node mapping by anionic polyelectrolytes, Biomaterials 32 (2011) 6551–6557, https://doi.org/10.1016/j.biomaterials.2011.05.039.
[54] J. Huarte, S. Espuelas, C. Martínez-Oharriz, J.M. Irache, Nanoparticles from Gantrez-based conjugates for the oral delivery of camptothecin, Int. J. Pharm. X 3 (2021) 100104, https://doi.org/10.1016/j.ijpx.2021.100104.
[55] A. Kumari, K. Kumari, S. Gupta, Protease responsive essential amino-acid based nanocarriers for near-infrared imaging, Sci. Rep. 9 (2019) 1–12, https://doi.org/10.1038/s41598-019-56871-4.
[56] A. Kumari, K. Kumari, S. Gupta, The effect of nanoencapsulation of ICG on two-photon bioimaging, RSC Adv. 9 (2019) 18703–18712, https://doi.org/10.1039/c9ra03152a.
[57] Z. Fatfat, M. Karam, B. Maatouk, D. Fahs, H. Gali-Muhtasib, Nanoliposomes as safe and efficient drug delivery nanovesicles, Adv. Mod. Approach. Drug Del. (2023) 159–197, https://doi.org/10.1016/B978-0-323-91668-4.00002-2.
[58] L.R. de Souza, L. Dourado, A. Silva, G. de Sousa, PVM/MA-shelled selol nanocapsules promote cell cycle arrest in A549 lung adenocarcinoma cells, J. Nanobiotechnol. 12 (2014) 1–17, https://doi.org/10.1186/s12951-014-0032-x.
[59] P.O. Ojer, L. Neutsch, F. Gabor, J.M. Irache, A.L. de Cerain, Cytotoxicity and cell interaction studies of bioadhesive poly(anhydride) nanoparticles for oral antigen/drug delivery, J. Biomed. Nanotechnol. 9 (2013) 1891–1903, https://doi.org/10.1166/jbn.2013.1695.
[60] L.A. Muehlmann, B.C. Ma, J.P.F. Longo, M.F.M.A. Santos, R.B. Azevedo, Aluminum–phthalocyanine chloride associated to poly(methyl vinyl ether-co-maleic anhydride) nanoparticles as a new third-generation photosensitizer for anticancer photodynamic therapy, Int. J. Nanomed. 9 (2014) 1199–1213, https://doi.org/10.2147/ijn.s57420.